ACS APPLIED NANO MATERIALS
Cite This: ACS Appl. Nano Mater. 2019, 2, 5272−5281
Article
www.acsanm.org

Graphene/Polyelectrolyte Layer-by-Layer Coatings for Electromagnetic Interference Shielding

Cristina Vallés,*,† Xiao Zhang,‡ Jianyun Cao,† Fei Lin,† Robert J. Young,† Antonio Lombardo,‡ Andrea C. Ferrari,‡ Laura Burk,§ Rolf Mülhaupt,§ and Ian A. Kinloch*,†

†School of Materials and National Graphene Institute, University of Manchester, Oxford Road, Manchester M13 9PL, U.K.
‡Cambridge Graphene Centre, University of Cambridge, 9 JJ Thomson Avenue, Cambridge CB3 0FA, U.K.
§Institute for Macromolecular Chemistry and Freiburg Materials Research Center FMF, Stefan-Meier-Straße, Freiburg, Germany

Supporting Information

ABSTRACT: Electromagnetic interference (EMI) shielding coating materials with thicknesses in the microscale are required in many sectors, including communications, medical, aerospace, and electronics, to isolate the electromagnetic radiation emitted from electronic equipment. We report a spray, layer-by-layer (LbL) coating approach to fabricate micrometer thick, highly ordered, and electrically conductive coatings with EMI shielding effectiveness (EMI SE ≥ 4830 dB/mm) through alternating self-assembly of negatively charged reduced graphene oxide (RGO) and a positively charged polyelectrolyte (PEI). The microstructure and resulting electrical properties of the $(PEI/RGO)_n$ LbL structures are studied as a function of increasing mass of graphene deposited per cycle (keeping the PEI content constant), number of deposited layers (n), flake diameter, and type of RGO. A strong effect of the lateral flake dimensions on the electrical properties is observed, which also influences the EMI SE. A maximum EMI SE of 29 dB is obtained for a 6 μm thick $(PEI/RGO)_{10}$ coating with 19 vol % loading of reduced electrochemically exfoliated graphene oxide flakes with diameters ∼3 μm. This SE performance exceeds those previously reported for thicker graphene papers and bulk graphene/polymer composite films with higher RGO or graphene nanoplatelets contents, which represents an important step toward the fabrication of thin and lightweight high-performance EMI shielding structures.

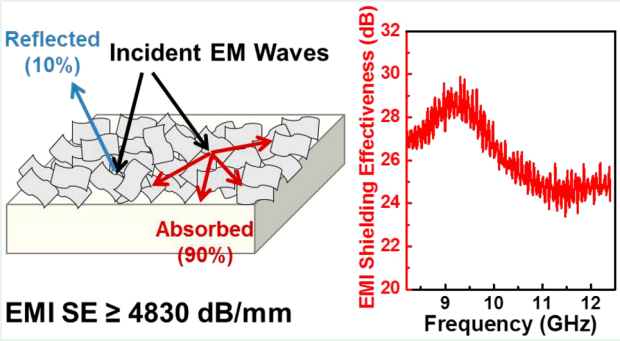

KEYWORDS: *graphene, layer-by-layer, coatings, electrical properties, electromagnetic interference (EMI) shielding*

INTRODUCTION

New environmental pollution problems[1] are emerging due to the rapid development of electronic technologies, including telephones, computers, and radios. Electronics and their components with higher power, smaller size, and faster operative speed emit unwanted electromagnetic waves, causing electromagnetic interference (EMI) between different electronic devices with detrimental impact on their performance.[2−5] Electrically conductive polymer composites can be used for EMI shielding[6−17] because of their lightweight, resistance to corrosion, flexibility, good processability, and low cost compared to conventional metal-based materials.[2] High electrical conductivity and connectivity of the conductive fillers in polymer composites are key factors to optimize their EMI shielding performance.[6,7,9,12,13] Carbon-based materials have been investigated as conductive fillers to fabricate composite materials for EMI shielding because they offer a combination of high electrical conductivity, excellent mechanical properties, lightweight, flexibility, and large aspect ratios.[6−17] In particular, graphene is promising for EMI shielding applications due to its excellent in-plane electrical conductivity (∼4.5 × 10^4 S/cm)[14,18−20] and easy processability.[21] Graphene-based polymer composites, foam structures, aerogels, thin films, and papers have already been investigated as lightweight EMI shielding materials.[2,22−30] An EMI specific shielding effectiveness (SSE, defined as signal attenuation in dB divided by density) ∼500 dB·cm^3/g was reported for a graphene foam composite with a density ∼0.06 g/cm^3,[2] and ∼33780 dB·cm^2/g for ultralight cellulose fiber/thermally reduced graphene oxide (RGO) hybrid aerogels, with a density as low as 2.83 mg/cm^3.[22] EMI shielding effectiveness (SE, defined as signal attenuation in dB) ∼21.8 dB was reported for a thermoplastic polyurethane/RGO composite foam with ∼3.17 vol % RGO,[27] whereas EMI SE ∼48.56 dB was found for 3D-interconnected graphene aerogels decorated with cobalt ferrite nanoparticles and ZnO nanorods.[28] Graphene papers with thicknesses between 12.5 and 470 μm[23,24] and ∼30−60 μm thick graphene/polymer composites[25,26] were also investigated as EMI shielding

Received: June 13, 2019
Accepted: June 24, 2019
Published: June 24, 2019

DOI: 10.1021/acsanm.9b01126
ACS Appl. Nano Mater. 2019, 2, 5272−5281

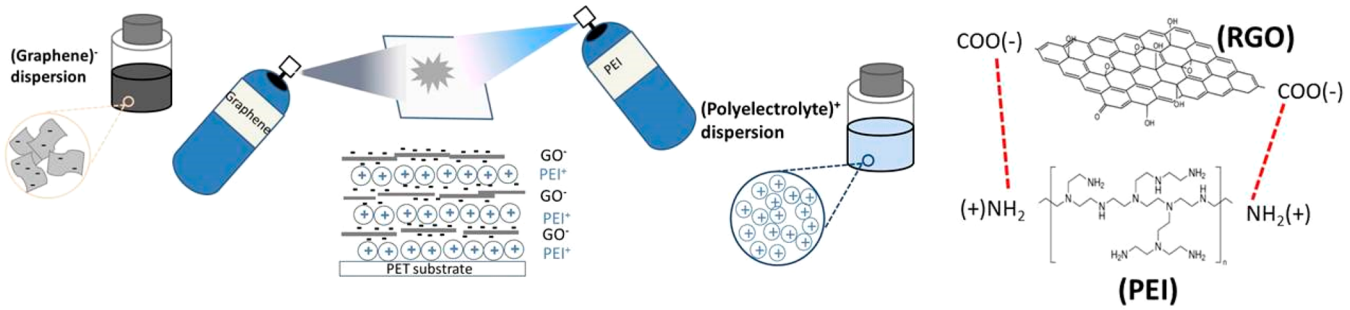

Figure 1. Schematic of the spray-coating approach used to fabricate the LbL coatings through alternating the absorption of negatively charged TRGO and a positively charged polyelectrolyte (PEI) on a PET substrate, to make $(PEI/TRGO)_n$ coatings (n = number of bilayers).

materials. Wan et al. reported EMI SE of up to ∼52.2 dB for iodine-doped and ∼47 dB for 12.5 μm thick undoped RGO papers,[23] whereas EMI SE ∼55.2 dB was reported for 0.47 mm multilayer films composed of highly ordered nitrogen-doped graphene.[24] EMI SE values up to 26 dB were reported for transparent films based on graphene nanosheets and silver nanowires,[29] and ∼58.5 dB for 6.6 μm thick nitrogen-doped graphene films.[30] EMI SE ∼14 dB was measured for 0.03−0.05 mm thick free-standing graphene/thermoplastic polyurethane (TPU) composite films with 0.12 volume fraction of liquid-phase-exfoliated graphene nanosheets,[25] whereas ∼27 dB was achieved for 0.35 mm thick multilayer graphene/polymer composite with 0.60 volume fraction of graphene.[26] Despite being required in sectors such as medical, aerospace, or electronics, micrometer thick graphene-based coatings with reduced graphene contents have not been exploited yet for EMI due to the difficulty to overcome the ∼20 dB target required for commercial applications[2] with low amounts of graphene (relative to most of the previously described works).

Layer-by-layer (LbL) assembly of oppositely charged polyelectrolytes and inorganic particles can be used to fabricate highly ordered multilayer nanostructured films and coatings with thickness in the nano or micro scale.[31] This coating method offers important advantages, such as uniform coverage of the substrate and controllable film/coating thicknesses.[31] Another advantage is its versatility, as it can be used with a variety of fabrication processes, including dip-, spray-, or spin-coating.[31] A few reports on the successful preparation of GO-polymer self-assembled multilayer structures using LbL approaches with gas barrier properties can already be found in the literature.[32−34] Transparent coatings/films prepared by LbL electrophoretic deposition of RGO[35] or by chemical vapor deposited (CVD) graphene alternated with spin-coated PMMA[36] were fabricated as transparent EMI shielding materials. In these works,[35,36] the LbL coatings were manufactured using dip-coating or electrophoretic deposition due to their ability to produce nanometer thick coatings with low graphene contents and hence high transparency.[35−37] However, for the majority of EMI applications, transparency is not required, allowing more scalable routes, such as spray coating, to be employed with high concentrations of graphene (≥10 wt %). Thus, a detailed evaluation of how the microstructure and electronic properties develop in LbL multilayered structures with increasing amounts of graphene is needed to optimize the properties of the coatings, while minimizing thickness, weight, and amount of graphene.

Here, we develop a spray LbL coating technique to fabricate up to 30 μm thick, electrically conductive graphene-based coatings on a substrate, alternating negatively charged RGO flakes and positively charged polyelectrolyte (PEI) to make $(RGO/PEI)_n$ coatings (n = number of deposition cycles), as schematically represented in Figure 1. We show how the microstructure, level of orientation of the graphene flakes, and electrical properties of the LbL coatings develop as a function of the amount of RGO deposited per cycle, while keeping the amount of PEI and n constant, and we relate it to their EMI SE. A maximum EMI SE of 29 dB was obtained for a 6 μm thick $(PEI/RGO)_{10}$ with 19 vol % loading of reduced electrochemically exfoliated GO flakes with diameters ∼3 μm, making our coatings promising for EMI shielding applications.

■ RESULTS AND DISCUSSION

Microstructure of the $(PEI/TRGO)_n$ LbL Coatings. Multilayered graphene coatings were prepared by using a LbL approach by alternating self-assembly of negatively charged thermally reduced GO (TRGO) and a positively charged polyelectrolyte (PEI), n times on a PET substrate, as represented schematically in Figure 1. The zeta potential was ∼−50 and −40 mV for 0.5 mg/mL dispersions of 100 μm-TRGO and 20 μm-TRGO, respectively, in ethanol, whereas a positive potential of ∼12 mV was found for a 10 mg/mL PEI/H_2O solution. The microstructure of the top surface and transverse section of the LbL $(PEI/TRGO)_n$ coatings was studied by SEM (details in the Experimental Section), and the micrographs are shown in Figure 2. The top surface has wrinkles (Figure 2a,b) similar to the topology of the TRGO flakes (TEM micrographs in Figure S1). This is consistent with a LbL formation where the particles dictate the morphology of the deposited polymer layers. SEM micrographs of the transverse sections of the LbL coatings in Figure 2c,d reveal that the spray-on approach produces highly ordered and well-defined multilayered microstructures.

To further characterize these coatings, polarized Raman spectroscopy was used. Polarized Raman spectroscopy was previously employed to evaluate and quantify the orientation of GO flakes in a PVA composite.[38] Following a procedure described by Li et al.,[38] the orientation of the TRGO flakes in the LbL coatings prepared here was evaluated by using a backscattering geometry and obtaining spectra with the polarized laser beam aligned either perpendicular (in the z-direction) or parallel (in the x-direction) to the surface as shown in Figure 3. The specimen was rotated relative to its axes, and an analyzer was used with the scattered light. A VV (vertical/vertical) combination of incident and scattered polarization was employed in which the directions of the incident and scattered polarization were the same, and the change in the intensity of the D band, I(D), with specimen

DOI: 10.1021/acsanm.9b01126
ACS Appl. Nano Mater. 2019, 2, 5272−5281

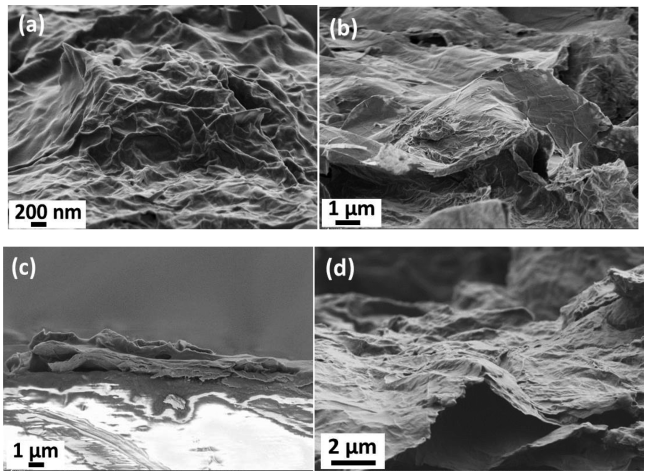

Figure 2. SEM images of the surface morphology of (PEI/20 μm-TRGO)$_5$ (a) and (PEI/100 μm-TRGO)$_5$ (b). SEM images of the transversal section of (PEI/20 μm-TRGO)$_5$ LbL coating (c, d) (TRGO loading = 14 vol %).

orientation was monitored. The I(D) variation for the two laser beam directions with the relative orientations of the incident laser polarization is shown in Figure 3. (The intensities were normalized to 1.) In the case where the laser beam is parallel to the z-axis (i.e., perpendicular to the plane of the coating, Φ_z) in Figure 3 it can be seen that I(D) remains approximately constant as the sample is rotated. In contrast, when the laser beam is parallel to the x-axis (Φ_x, Figure 3), I(D) is a maximum when the direction of laser polarization is parallel to the sample edge plane and aminimum when it is perpendicular to the edge.[39] This is consistent with the in-plane alignment of the TRGO layers in the LbL coating structure seen in the SEM micrograph in Figure 2.

A fitting of the data in Figure 3 follows

$$\mathrm{I(D)} = A \cos^4 \Phi_x + B \tag{1}$$

with $A = 0$ and $B = 1$ for randomly oriented flakes and $A = 1$ and $B = 0$ for a perfect alignment. A higher level of orientation (i.e., a higher A and a lower B; see Figure 3) is detected in coatings with 10.8 vol % graphene than with 24 and 38 vol %, for the same n. This may be due to a combination of more overlap between flakes and the formation of small agglomerates of graphene at higher loadings. The former is related to the onset of in-plane coverage, meaning that the 24 and 38 vol % coatings have similar levels of orientation (see later), while the latter is consistent with Li's work[38] where a decreasing orientation with increasing GO loading was observed in PVA composites and attributed to aggregation.

All samples have a similar crumpled surface morphology (Figures 2a,b) and multilayered structure (transverse surface, Figures 2c,d). Their thicknesses (shown in Figure S4)

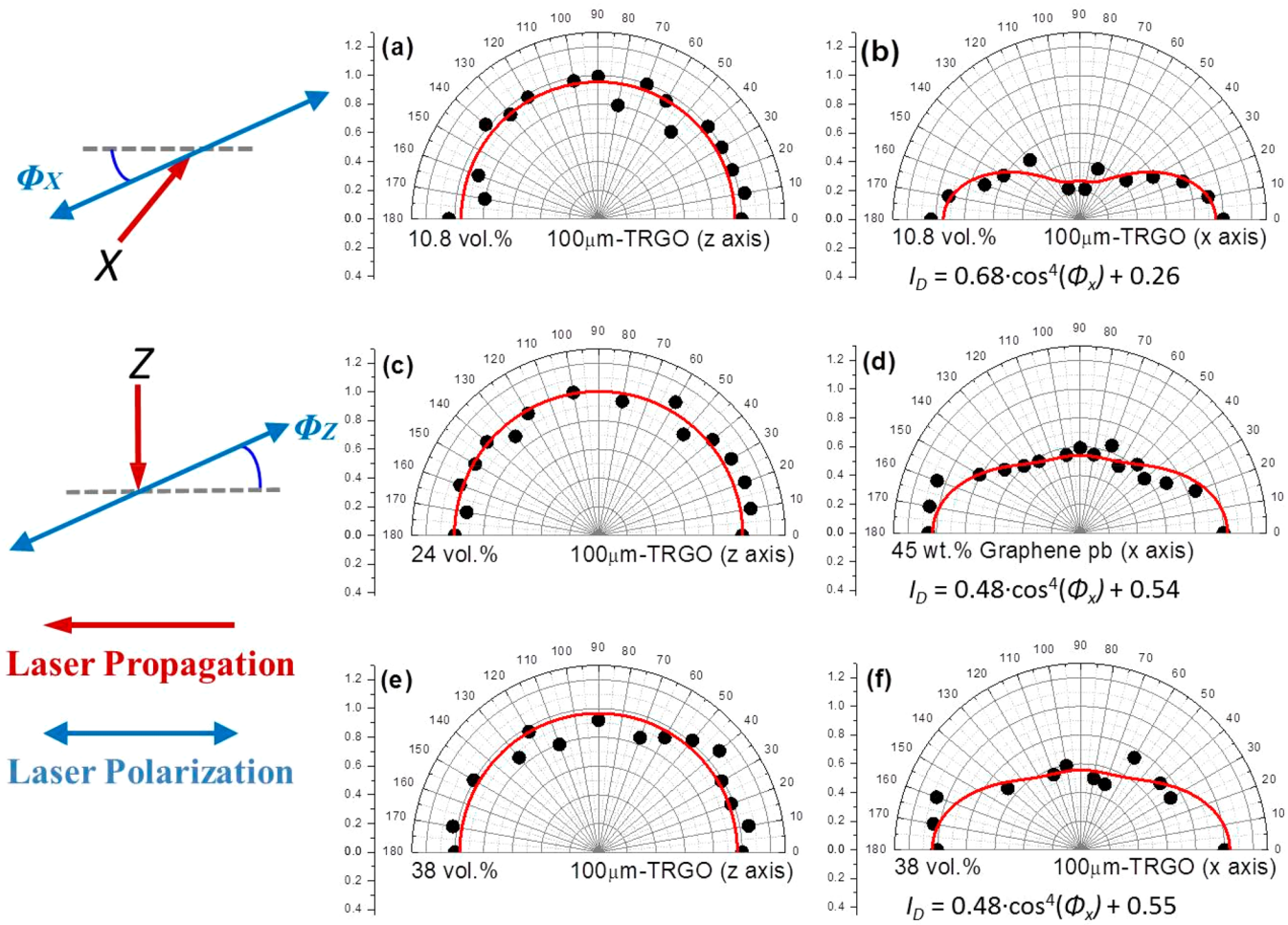

Figure 3. I(D) variation as a function of Φ_z (a, c, e) and Φ_x (b, d, f) for (PEI/100 μm-TRGO)$_{10}$ coatings with different graphene loadings.

DOI: 10.1021/acsanm.9b01126
ACS Appl. Nano Mater. 2019, 2, 5272−5281

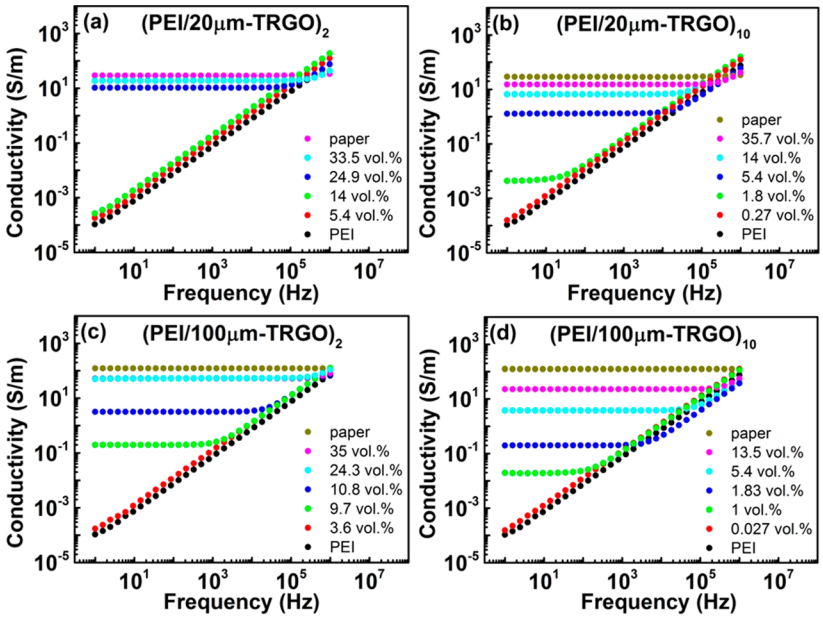

Figure 4. Log−log plots of conductivity as a function of frequency for (PEI/20 μm-TRGO)$_n$ and (PEI/100 μm-TRGO)$_n$ LbL coatings (n = 2, n = 10) for different graphene loadings.

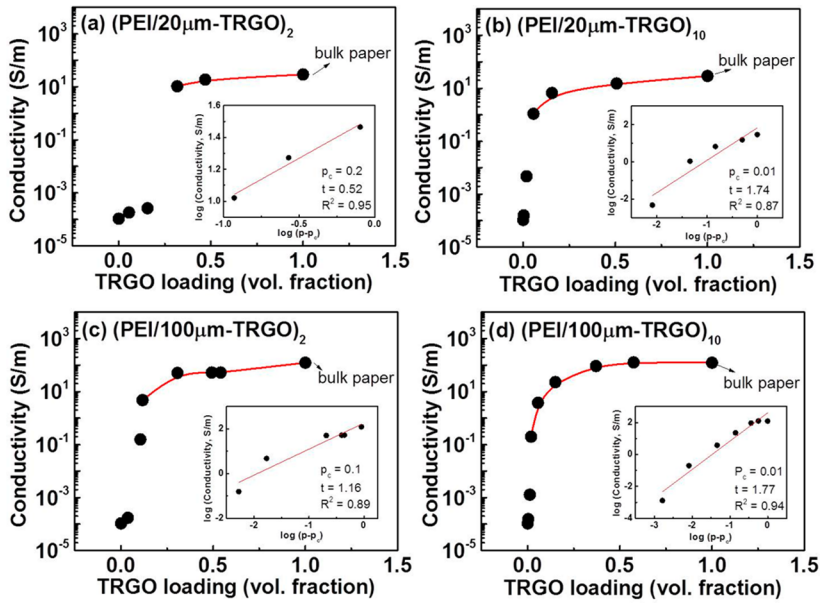

Figure 5. Semilog plot of conductivity as a function of graphene loading for LbL-coated systems: (a) (PEI/20 μm-TRGO)$_2$; (b) (PEI/20 μm-TRGO)$_{10}$; (c) (PEI/100 μm-TRGO)$_2$; (d) (PEI/100 μm-TRGO)$_{10}$. The insets are log−log plots of conductivity as a function of $P - P_c$, determined from the volume fraction data.

depended on loading and n as well as on flakes lateral dimensions. The loading, i.e., the amount of graphene deposited per cycle, can be controlled by modifying the volume of a dispersion of graphene with a known concentration. A linear increase of the overall thickness with increasing loading is observed for constant n. At very low loadings (<0.027 vol %) similar thicknesses were observed for 20 and 100 μm diameter flake (named 20 μm-TRGO and 100 μm-TRGO, respectively) based coatings as expected from depositing TRGO flakes with similar thicknesses, whereas the coatings fabricated with the 100 μm-TRGO are thicker at higher loadings, probably due to increased overlap of large flakes relative to the small flakes. The thicknesses of the coatings increase with n for constant graphene loading.

Electrical Properties. To understand how the electrical conductance develops in multilayer microstructures, the conductivity of LbL coating structures was evaluated with increasing loading per cycle and n. The log−log plots of conductivity as a function of frequency for (PEI/20 μm-TRGO)$_n$ and (PEI/100 μm-TRGO)$_n$ at increasing loading of graphene for n = 2 and n = 10 are plotted in Figure 4. Figure 4 shows the behavior typical of two-phase systems, i.e., a resistive component (GO) and a capacitive component (PEI, i.e., a dielectric material). Below the percolation threshold, the conductivity depends linearly on frequency, as characteristic of

DOI: 10.1021/acsanm.9b01126
ACS Appl. Nano Mater. 2019, 2, 5272−5281

Table 1. Experimental and Theoretically Calculated Percolation Thresholds and Coverage Graphene Loadings for the LbL Coatings

graphene	n	exp. perc. threshold	theor. perc. threshold[a]	exp. coverage[b]	theor. coverage[c]
20 μm-TRGO	2	0.20	0.0013−0.0037 (vol. fraction)	0.24 (vol. fraction)	0.002−0.0059 (vol. fraction)
	10	0.01			
100 μm-TRGO	2	0.10			
	10	0.01			

[a]Graphene fraction corresponding to 68% area occupation. [b]Corresponding to the transition from n-dependency to n-independency. [c]Calculations shown in theSupporting Information (fraction of graphene corresponding to an area occupation of 1).

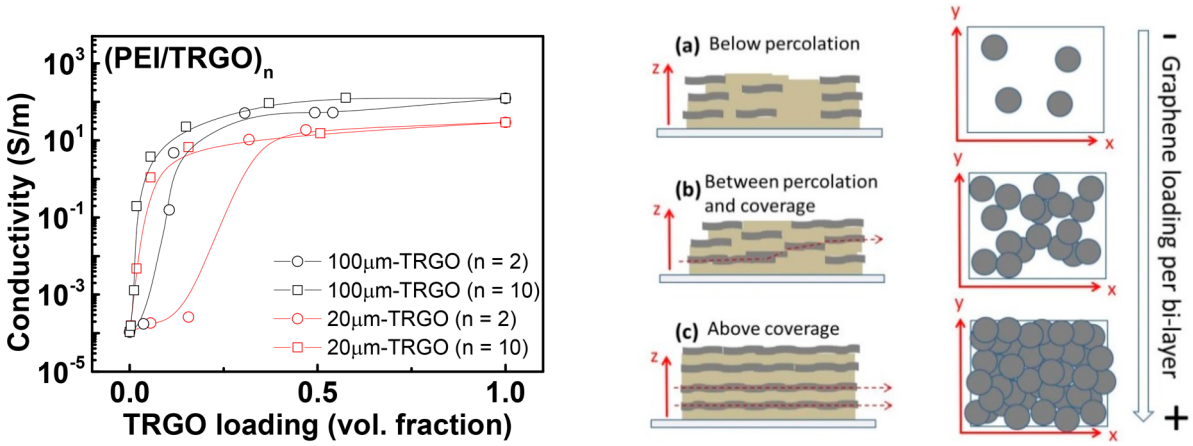

Figure 6. Comparison of the conductivity of (PEI/20 μm-TRGO)$_n$ and (PEI/100 μm-TRGO)$_n$ LbL coatings for different n and schematic representation of the three electrical behavior regimes for LbL coatings with increasing graphene loading: (a) below percolation; (b) between percolation and coverage (conductivities are n-dependent); (c) above coverage (conductivities are n-independent).

dielectric behavior, and typical of insulating materials.[40] Above percolation the conductivity plateaus up to a critical frequency at which the behavior reverted to a dielectric behavior. This indicates the formation of conductive paths within the matrix and a dominance of the resistive component, combined with a dielectric behavior at higher frequencies where the capacitive component (i.e., the polyelectrolyte and network junctions) dominates. At high loadings (>13.5 vol % for n = 2 and >24.3 vol % for n = 10) the conductivity is independent of frequency across the entire frequency range. This is typical of an electrically conductive material,[40] similar to that observed for a pure graphene paper (i.e., afree-standing paper prepared by vacuum filtration of a dispersion of the as-prepared graphene), also shown in Figure 4.

Percolation Threshold. The percolation threshold depends on the flakes lateral dimensions and n. For the (PEI/20 μm-TRGO)$_n$ systems the percolation is between ∼14 and 25 vol % of graphene for n = 2 and between 0.3 and 1.8 vol % for n = 10. For LbL coatings with 100 μm-TRGO this is in the ranges of 3.6−9.8 and 0.2−1.2 vol % for n = 2 and n = 10, respectively. Figure 5 shows the conductivities of the LbL structures at 1 Hz as a function of graphene loading for the two graphene types studied here at n = 2, 10. These show S-shaped curves typical of percolated systems,[40] suggesting that classical percolation theory[41] could be used to calculate the percolation threshold (P_c), defined as the critical/minimum amount of filler required to transform a nonconductive material into a conductive one. Assuming that the fillers are distributed randomly within the polymer matrix, the conductivity can be described as[40]

$$\sigma = \sigma_0(P - P_c)^t \quad (2)$$

where P is the fraction of filler in the LbL structure, P_c is the percolation threshold, t is the conductivity exponent, σ_0 is the electrical conductivity of the matrix, and σ is the electrical conductivity of the LbL system.

From Figure 5, P_c = 0.20 for n = 2 and P_c = 0.01 were determined for n = 10 for (PEI/20 μm-TRGO)$_n$. Linear fittings of log(conductivity) vs log($P - P_c$) data (inset in Figure 5) give t = 0.52 and 1.74 for n = 2, 10, respectively. Similarly, for the (PEI/100 μm-TRGO)$_n$, P_c = 0.10 for n = 2 and P_c = 0.01 for n = 10 were found, resulting in t = 1.16 and 1.77, respectively.

Lower percolation thresholds were found for 100 μm- than for 20 μm-TRGO for identical graphene loading and n. Also, the percolation threshold for n = 10 is lower than for n = 2 (for identical loading of graphene and independent of the lateral dimensions). The percolation thresholds are summarized in Table 1.

Pike and Seager[42] studied a two-dimensional random-lattice site system at a critical area fraction of ∼0.68 using Monte Carlo calculations and assuming particles to be uniform discs with hard cores. If we consider the TRGO flakes as uniform discs deposited on a substrate (in one deposition cycle) with overlapping, the percolation should happen theoretically at 0.0013−0.0037,[42] which corresponds to the volume fraction of graphene calculated for one deposition cycle with the graphene occupying 68% of the surface of the substrate (see Supporting Information). The theoretical values are lower than those derived from our experiments, which we assign to the presence of defects on the TRGO flakes coming from the reduction process, the presence of gaps possibly associated with an inhomogeneous distribution of flakes, and the fact that TRGO flakes are not discs with uniform diameters. The wrinkled

DOI: 10.1021/acsanm.9b01126
ACS Appl. Nano Mater. 2019, 2, 5272−5281

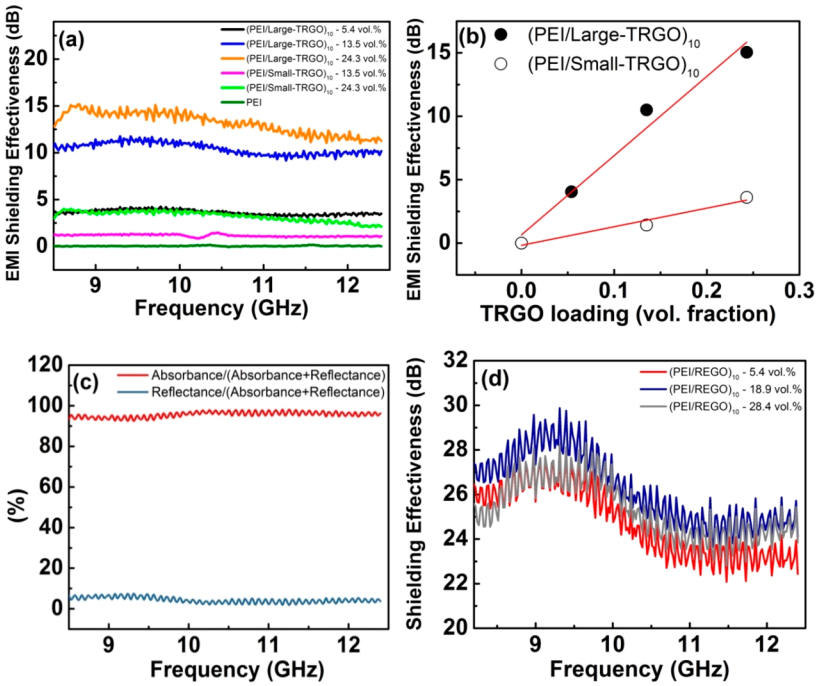

Figure 7. (a) Total EMI SE of (PEI/100 μm-TRGO)$_n$ and (PEI/20 μm-TRGO)$_n$ LbL coating structures. (b) EMI SE vs volume fraction of TRGO. A linear fit to the data gives: EMI SE (dB) = 14.63·vol (R^2 = 0.93) and EMI SE (dB) = 62.47·vol (R^2 = 0.97) for (PEI/20 μm-TRGO)$_{10}$ and (PEI/100 μm-TRGO)$_{10}$, respectively. (c) Absorbance/(absorbance + reflectance) and reflectance/(absorbance + reflectance) contributions. (d) Total EMI SE of (PEI/REGO)$_{10}$ LbL coating.

nature of TRGO flakes (TEM, Supporting Information) may also contribute to this discrepancy.

For a percolated system, t depends on the dimensionality of the composites. Theoretically, t should vary from ~1.6 to 2.0 for three dimensional (3D)-percolated systems and from 1 to ~1.6 for two dimensional (2D).[40,43] Applying the classical percolation theory[42] to our data, we can say that our LbL coatings show a 2D-percolation mechanism, with t increasing with n, which suggests an evolution from 2D- to 3D-percolated systems from n = 2 to n = 10. In addition, higher values of t are found for larger flakes, as expected from percolation theory.[40]

Zhao et al.[44] studied percolation in graphitic conductive networks embedded in polymer composites and reported t = 2.40−6.92, corresponding to 3D-percolation. Du et al.[45] reported t = 1.08 for a 2D-percolated segregated graphene network in bulk high-density polyethylene composites processed by a hot press, which suggests that the level of orientation/organization of the fillers in the matrix must be defining the dimensionality of conduction. We thus assign the level of organization achieved in our LbL coatings (evidenced by SEM and polarized Raman) as responsible for the 2D conduction mechanism found here. The differences between theory and experimental data, and the discrepancies between different reported experimental systems, might be related to additional factors influencing percolation, such as additional dimensional aspects of the filler network, presence of agglomerates, polymer−filler interaction, and level of organization/orientation.

Development of the Conductance in LbL Structures above Percolation. Above percolation, the conductivities increase with graphene loading and n up to a maximum limit (Figure 6). The n-dependence before saturation suggests that when the electrons find defects or gaps in one graphene layer, they tend to hop to the next level (from n = 1 to n = 2, ..., as schematically represented in Figure 6), leading to enhancement of overall conductivities (the variation of the conductivities of the coatings with increasing n is shown in Figure S6). This observation agrees with the small increase in t with increasing n, i.e., the increasing 3D nature of the network. Even with the electrons hopping to contiguous layers to find more conductive paths, the systems behave as 2D-percolated systems.

Coverage. There is a second critical graphene loading at which conductivities reach a maximum (Figure 6). This maximum cannot be further increased, neither by increasing graphene loading nor by increasing n, and corresponds to the conductivity measured for bulk papers composed purely of graphene (i.e., the inherent conductivity of graphene employed for the fabrication of the LbL structures where the interflake resistance gives an intrinsic limit).

We attribute the transition from n-dependency to n-independency to the formation of a continuous network of graphene in one deposition cycle, which we define as *complete coverage* (i.e., 100% occupation of the surface). The experimental coverage loading is found at a volume fraction ~0.24, significantly higher than the theoretical loading (calculations shown in the Supporting Information), similar to what we observed for the percolation and due to the same reasons (the theoretical coverage volume fraction of graphene is estimated as ~0.001−0.0032).

Figure 3 reveals lower orientation at volume fractions of TRGO ≥ 0.24 (i.e., above complete coverage), related to the presence of more wrinkles and overlapping between flakes above coverage relative to a situation in which "isolated" TRGO flakes are deposited with not many connections, overlaps, or agglomerates (as represented schematically in Figure 6). All experimental and theoretically calculated percolation thresholds and graphene loadings are compiled

DOI: 10.1021/acsanm.9b01126
ACS Appl. Nano Mater. 2019, 2, 5272−5281

Table 2. Comparison between the EMI SE Data Found in This Work and Previously Reported Data for Graphene Papers and Graphene/Polymer Composite Films

material	EMI SE (dB)	thickness (mm)	volume fraction graphene	dB/mm	ref
LbL $(TRGO/PEI)_n$ coatings	15	0.03	0.30	500	this work
LbL $(R\text{-}EGO/PEI)_n$ coatings	29	≤0.006	0.30	≥4830	this work
graphene paper	47−52.2	0.0125	1	3760−4176	23
N-doped graphene paper	55.2	0.47	1	117.4	24
graphene/TPU film	14	0.03−0.05	0.12	280−466	25
graphene/epoxy	27	0.04−0.06	0.6	675−450	26
RGO-EDA	58.5	0.0066	1	8863	30

in Table 1. (The percent coverage corresponding to the fractions studied here is presented in the Supporting Information.)

At graphene loadings above complete coverage, interlayer hopping no longer provides paths of higher conductivity. Hence, the conductivity becomes independent of n and maximum conductivities of 19 S/m for 34 vol % of 20 μm-TRGO and 127 S/m for 39 vol % of 100 μm-TRGO are found. The maximum conductivity corresponds to the conductivity of a graphene paper, highlighting the importance of choosing an electrically conductive filler, as required for the targeted application, but with sufficient charged groups for LbL formation.

Reaching coverage in one deposition cycle is an important parameter to optimize the electrical properties while minimizing thickness and graphene loading. Within the n-dependent region the coatings are typically thicker and less conductive than those fabricated with just one deposition cycle using graphene loadings above coverage. Most of the reported work[46,47] on multilayered structures did not achieve coverage in one deposition cycle, typically focusing on increasing conductivities by incrementing the number of deposition cycles until saturation. In the works reported by D. G. Wang et al.[46]and L. Wang et al.[47] electrons were assumed to hop between layers, in agreement with our results below coverage (shown in Figure S6).

The self-assembly of 100 μm-TRGO flakes gives higher conductivities and lower percolation thresholds relative to those found for self-assembly of 20 μm-TRGO for identical n, which we relate to the presence of more flake−flake connections and defects in 20 μm- than in 100 μm-TRGO (also observed for the bulk papers). Previously reported simulations and experiments showed that fillers with larger aspect ratios lead to reduced percolation thresholds in systems with higher dimensionalities.[48−50]

EMI Shielding. The coatings with the largest amounts of graphene materialand the highest electrical conductivities were then EMI tested. Figure 7 plots the EMI SE for $(PEI/TRGO)_{10}$ LbL structures prepared with increasing graphene in the range of 8−13 Hz, widely used in communication applications such as TV, microwaves, and telephones.[51] Figure 7a indicates that the EMI SE is almost constant across the entire range of frequencies. These data reveal that EMI SE increases linearly with increasing graphene loadings for a constant n. The data can be linearly fitted (Figure 7b), indicating higher EMI SE with increasing graphene content.

A strong effect of the lateral dimensions of TRGO flakes on the EMI SE is also observed, related to the superior electrical properties of the larger TRGO flakes relative to the smaller ones. These results are in agreement with the work by Wan et al.[23] where superior EMI shielding was reported for larger size graphene sheets. These authorsalso attributed this finding to fewer defects and a more conjugated carbon domain size in larger flakes, leading to higher electrical conductivities and, thus, to superior EMI SE.

To establish a basis for designing high-performance EMI shielding materials, we consider the mechanism for improved EMI shielding performance was investigated.Figure 7 plots absorbance/(absorbance + reflectance) and reflectance/(absorbance + reflectance) contributions to the total EMI SE for a $(PEI/100\ \mu m\text{-}TRGO)_{10}$ coating. This shows a 10% contribution of reflectance and a 90% absorbance, indicating that absorption is the dominant shielding, in agreement with previously reported works.[23,36]

Our LbL coating approach can also be used for other negatively charged graphene materials, such as hydroiodic acid (HI)-reduced electrochemically exfoliated GO (EGO).[52]Zeta-potential of ∼−45 mV for a 1 mg/mL aqueous dispersion of EGO, and its electrical conductivity is much higher than TRGO. The variation of sheet resistance of LbL coatings with increasing graphene loading is shown in Figure S8. The maximum conductivity (i.e., minimum sheet resistance) depends on the type of graphene (level of defects and inherent conductivity), which suggests the possibility of improving and tuning the electrical properties of the coatings by using graphene materialswith lower amount of defects and, thus, higher conductivities. As a consequence, the total EMI SE of these reduced electrochemically produced graphene-based coatings (Figure 7d) is ∼5 times higher than TRGO-based coatings with similar graphene content and n. In addition, the $(PEI/R\text{-}EGO)_n$ coatings are thinner than those prepared by using TRGO, which makes these EMI SE better in terms of dB/mm (see Table 2 for comparison with literature data on graphene-based papers and graphene/polymer composite films). We get EMI SE ∼29 dB for ∼6 μm thick samples (SEM micrograph, Figure S9). These results suggest that our approach can be used for other processable graphene materials (provided they have negatively charged surfaces), which offers the possibility of tuning electrical conductivity and EMI SE to fit the requirements of emerging applications.

The maximum EMI SE per unit thickness in $(PEI/100\ \mu m\text{-}TRGO)_{10}$ LbL coating (500 dB/mm) and R-EGO based coating (4830 dB/mm) compare favorably with the literature. Wan et al.[23] reported EMI SE values of up to ∼52.2 dB for iodine-doped graphene papers and ∼47.0 dB for undoped graphene papers with thicknesses ∼12.5 μm. A similar EMI SE (∼55.2 dB) was reported for multilayer films of highly ordered nitrogen-doped graphene with a much higher thickness (0.47 mm),[24] whereas the work by Lin et al.[30] reported slightly higher EMI SE values for nitrogen-doped graphene papers with higher total amounts of graphene. Thus, our LbL coatings have better EMI shielding with lower graphene content (Table 2).

DOI: 10.1021/acsanm.9b01126
ACS Appl. Nano Mater. 2019, 2, 5272−5281

Our EMI SE are also superior to most previously studied graphene/polymer composites, typically using higher graphene contents.[25,26] Our results are better than those reported by Song et al.[26] (EMI SE up to ∼27 dB) for much thicker (0.35 mm) films of multilayer graphene/epoxy composite containing 0.60 volume fraction of graphene as well as better than the EMI SE ∼14 dB reported for free-standing conducting graphene/TPU composite films with 0.12 volume fraction of graphene and thicknesses between 0.03 and 0.05 mm.[25] Thin coatings/films prepared by LbL electrophoretic deposition of RGO[35] or by CVD graphene alternated with spin-coated PMMA[36] were fabricated as transparent EMI shielding materials. Although they exhibited high dB/mm (2−3 orders of magnitude higher than ours), the absolute EMI SE values are limited by the transparency required in some sectors. We did not focus on fabricating transparent coatings, but on increasing the absolute EMI SE. Our method allows us, thus, to fabricate bulk (i.e., nontransparent) structures but still thin (up to 30 μm thick) and highly ordered graphene-based coatings to maximize the electrical conductivity and EMI SE with the minimum thickness and amount of graphene employed. This underlines the importance of designing highly ordered structures with optimized electrical properties to maximize EMI shielding, minimizing both thickness and graphene content.

■ CONCLUSIONS

We report here a scalable spray coating layer-by-layer approach to fabricate thin, highly ordered, and electrically conductive multilayer coatings for EMI shielding, through alternating self-assembly of negatively charged RGO and apositively charged polyelectrolyte*n* times on a substrate to fabricate $(PEI/RGO)_n$ coatings. SEM micrographs of the transverse sections of the LbL coatings revealed highly ordered and well-defined multilayered microstructures, with thicknesses depending on the loading of graphene per bilayer and *n*. Percolation theory was applied to these structures to understand the conduction mechanism. Outstanding EMI shielding performances were found for these coating structures through a mechanism of absorption. Maximum values of EMI SE ∼29 dB for 6 μm thick coatings with 19 vol % loading of reduced electrochemically produced graphene oxide were found, considerably higher than those previously reported for thicker graphene papers and graphene/polymer composites with higher graphene contents, making our coatings promising for EMI shielding applications in sectors where high EMI SE is important (especially if EMI absorbance is required) while transparency is not needed. In addition, we showed that the EMI shielding performance of graphene-based structures can be tuned by varying the nature and electrical properties of the graphene employed.

■ EXPERIMENTAL SECTION

Preparation and Characterization of TRGO and R-EGO. To remove oxygen-containing functionalities from the surface of the flakes, GO powder (prepared by using Hummers' method) was thermally reduced in a nitrogen atmosphere by a rapid heating up to 750 °C using a metallic reactor heated with a gas burner.[53] TRGO was obtained as a black powder of very low bulk density. The superheating is the prime requirement to achieve exfoliation of graphite simultaneously to the reduction. To control the diameter of the TRGO, two types of starting graphite were employed. A micrographite with a particle size distributiond_{50} = 17−23 μm (SGA 20 M 99.5; AMG graphite, Hauzenberg, Germany) was used to prepare TRGO with a particle size distribution between 5 and 200 μm and an average diameter of ∼20 μm (20 μm-TRGO). Graphite with larger particles (Rfl 99.5; AMG graphite, Hauzenberg, Germany; min 90% > 160 μm) was employed to produce TRGO with a particle size between 5 and 900 μm and d_{50} ∼ 100 μm (100 μm-TRGO).

The combination of different average diameters (∼20 μm vs ∼100 μm characteristic of 20 μm-TRGO and 100 μm-TRGO flakes, respectively, as revealed by TEM, Supporting Information) and similar thicknesses (between 3.5 and 10 nm as revealed by AFM Supporting Information) makes these materials ideal to evaluate the role of the lateral flake dimensions on the microstructure and properties of the LbL coatings. (Further characterization of the TRGO filler materials, including XPS showing reduction, is in Supporting Information.)

Electrochemically exfoliated graphene oxide (EGO) was prepared following the experimental procedure reported elsewhere.[52] For the EGO-based LbL coatings, the reduction was performed after deposition (as described below).

Preparation of the LbL Structures. Multilayered graphene coatings are prepared by using a LbL approach by alternating self-assembly of negatively charged TRGO and positively charged PEI, *n* times on a PET substrate, as represented schematically in Figure 1. A commercial aerosol (Linden H-BADG-AIRBRUSH-KIT) was used to deposit graphene and PEI by spraying the dispersions of TRGO in ethanol and the aqueous solutions of PEI, alternatively, on a PET substrate. The coatings were dried using an air flow at room temperature after each deposition. The effect of rinsing after each is discussed in the Supporting Information.

To assess the formation of the LbL system, the amount of graphene deposited per cycle (i.e., mg of graphene per deposition cycle and unit surface area, defined here as "areal mass of graphene") is varied while the areal mass of PEI is kept constant (= 0.18 mg/cycle/cm^2). The areal masses of TRGO and PEI are used to calculate the loading of graphene in the LbL structures as a weight per unit volume fraction. The loading depends on the areal masses of graphene and PEI (consequently, "graphene loading per cycle" is equivalent to just "graphene loading") but is independent of *n*. To assess the interaction between layers, *n* is varied between 1 and 10. The graphene loading, i.e., the amount of graphene deposited per cycle, can be controlled accurately by modifying the deposited volume of a dispersion of graphene with a known concentration. In a similar way, the final thickness of the fabricated coatings can be also controlled accurately through controlling the graphene deposited per cycle and *n*.

For the preparation of the R-EGO-based LbL coatings, the EGO (prepared following the method reported elsewhere)[52]was first deposited from a 1 mg/mL aqueous dispersion (with ∼−45 mV zeta potential). After deposition, the LbL EGO coatings were placed in a sealed bottle (100 mL in volume), containing 0.5 mL of HI (55%) and 1.25 mL of acetic acid, in a water bath at 95 °C for 1 h for reduction. The reduced EGO (R-EGO) coatings were rinsed with ethanol four times to remove any residual acid and iodine and dried with N_2gas.

Characterization. A Zeiss Ultra 55 FEG-SEM (scanning electron microscope) is employed to analyze the surface morphology and the transversal section of the LbL coatings (using a EHT of 2 kV).

The sample thicknesses are measured with a digital micrometer IP65 QUANTUMIKE. The impedance is tested on 2 mm × 3 mm specimens using a PSM 1735 frequency response analyzer from Newtons4th Ltd. connected with the impedance analysis interface (IAI) at the range of frequencies from 1 to 10^6 Hz. The conductivities (σ) of the coatings are calculated from the measured impedances as[40]

$$\sigma(\omega) = |Y^*(\omega)|\frac{t}{A} = \frac{1}{Z^*}\frac{t}{A} \tag{3}$$

where $Y^*(\omega)$ is the complex admittance, Z^* is the complex impedance, and t and A are the thickness and cross section area of the sample.

An Evolution 201 Thermo Scientific UV−vis spectrophotometer is employed to analyze the absorption and transmittance in the range 300−800 nm. EMI shielding tests are performed using a PNA (vector network analyzer 10 MHz−50 GHz), two RF cables, and one pair of

DOI: 10.1021/acsanm.9b01126
ACS Appl. Nano Mater. 2019, 2, 5272−5281

waveguides in the X-band frequency range (8.4−12.4 GHz). The samples (2.5 × 1.5 cm^2 coatings) are compressed in the middle of two waveguides while VNA measured the S_{21} (transmittance), from which SE is calculated.

■ ASSOCIATED CONTENT

Supporting Information

The Supporting Information is available free of charge on the ACS Publications website at DOI: 10.1021/acsanm.9b01126.

Details of fabrication, characterization, and calculations (PDF)

■ AUTHOR INFORMATION

Corresponding Authors

*E-mail: cristina.valles@manchester.ac.uk.

*E-mail: ian.kinloch@manchester.ac.uk.

ORCID

Cristina Vallés: 0000-0002-9359-1705

Jianyun Cao: 0000-0003-3437-9947

Robert J. Young: 0000-0001-6073-9489

Antonio Lombardo: 0000-0003-3088-6458

Andrea C. Ferrari: 0000-0003-0907-9993

Ian A. Kinloch: 0000-0003-3314-6869

Notes

The authors declare no competing financial interest.

■ ACKNOWLEDGMENTS

We acknowledge funding from the EU Graphene Flagship, EU Grant Neurofibres, ERCs grants Hetero2D and MINER-GRACE, EPSRC grants EP/L016087/1, EP/K01711X/1, EP/N010345/1, EP/K017144/1, EP/P02081X/1.

■ REFERENCES

(1) Shahzad, F.; Alhabeb, M.; Hatter, C. B.; Anasori, B.; Hong, S. M.; Koo, C. M.; Gogotsi, Y. Electromagnetic interference shielding with 2D transition metal carbides (MXenes). *Science* **2016**, *353*, 1137−1140.

(2) Chen, Z. P.; Xu, C.; Ma, C. Q.; Ren, W. C.; Cheng, H. M. Lightweight and Flexible Graphene Foam Composites for High-Performance Electromagnetic Interference Shielding. *Adv. Mater.* **2013**, *25*, 1296−1300.

(3) Yan, D. X.; Pang, H.; Li, B.; Vajtai, R.; Xu, L.; Ren, P. G.; Wang, J. H.; Li, Z. M. Structured Reduced Graphene Oxide/Polymer Composites for Ultra-Efficient Electromagnetic Interference Shielding. *Adv. Funct. Mater.* **2015**, *25*, 559−566.

(4) Yousefi, N.; Gudarzi, M. M.; Zheng, Q.; Lin, X.; Shen, X.; Jia, J.; Sharif, F.; Kim, J. K. Highly aligned, ultralarge-size reduced graphene oxide/polyurethane nanocomposites: Mechanical properties and moisture permeability. *Composites, Part A* **2013**, *49*, 42−50.

(5) Zhang, Y.; Huang, Y.; Zhang, T. F.; Chang, H. C.; Xiao, P. S.; Chen, H. H.; Huang, Z. Y.; Chen, Y. S. Broadband and Tunable High-Performance Microwave Absorption of an Ultralight and Highly Compressible Graphene Foam. *Adv. Mater.* **2015**, *27*, 2049−2053.

(6) Yang, Y.; Gupta, M. C.; Dudley, K. L.; Lawrence, R. W. Novel carbon nanotube-polystyrene foam composites for electromagnetic interference shielding. *Nano Lett.* **2005**, *5*, 2131−2134.

(7) Chung, D. D. L. Electromagnetic interference shielding effectiveness of carbon materials. *Carbon* **2001**, *39*, 279−285.

(8) Geetha, S.; Kumar, K. K. S.; Rao, C. R. K.; Vijayan, M.; Trivedi, D. C. EMI Shielding: Methods and Materials-A Review. *J. Appl. Polym. Sci.* **2009**, *112*, 2073−2086.

(9) Zhang, H. B.; Yan, Q.; Zheng, W. G.; He, Z. X.; Yu, Z. Z. Tough Graphene-Polymer Microcellular Foams for Electromagnetic Interference Shielding. *ACS Appl. Mater. Interfaces* **2011**, *3*, 918−924.

(10) Eswaraiah, V.; Sankaranarayanan, V.; Ramaprabhu, S. Functionalized Graphene-PVDF Foam Composites for EMI Shielding. *Macromol. Mater. Eng.* **2011**, *296*, 894−898.

(11) Fletcher, A.; Gupta, M. C.; Dudley, K. L.; Vedeler, E. Elastomer foam nanocomposites for electromagnetic dissipation and shielding applications. *Compos. Sci. Technol.* **2010**, *70*, 953−958.

(12) Thomassin, J. M.; Pagnoulle, C.; Bednarz, L.; Huynen, I.; Jerome, R.; Detrembleur, C. Foams of polycaprolactone/MWNT nanocomposites for efficient EMI reduction. *J. Mater. Chem.* **2008**, *18*, 792−796.

(13) Li, N.; Huang, Y.; Du, F.; He, X. B.; Lin, X.; Gao, H. J.; Ma, Y. F.; Li, F. F.; Chen, Y. S.; Eklund, P. C. Electromagnetic interference (EMI) shielding of single-walled carbon nanotube epoxy composites. *Nano Lett.* **2006**, *6*, 1141−1145.

(14) Liang, J. J.; Wang, Y.; Huang, Y.; Ma, Y. F.; Liu, Z. F.; Cai, J. M.; Zhang, C. D.; Gao, H. J.; Chen, Y. S. Electromagnetic interference shielding of graphene/epoxy composites. *Carbon* **2009**, *47*, 922−925.

(15) Liu, Z. F.; Bai, G.; Huang, Y.; Ma, Y. F.; Du, F.; Li, F. F.; Guo, T. Y.; Chen, Y. S. Reflection and absorption contributions to the electromagnetic interference shielding of single-walled carbon nanotube/polyurethane composites. *Carbon* **2007**, *45*, 821−827.

(16) Wang, L. L.; Tay, B. K.; See, K. Y.; Sun, Z.; Tan, L. K.; Lua, D. Electromagnetic interference shielding effectiveness of carbon-based materials prepared by screen printing. *Carbon* **2009**, *47*, 1905−1910.

(17) Yang, Y. L.; Gupta, M. C.; Dudley, K. L.; Lawrence, R. W. Conductive carbon nanoriber-polymer foam structures. *Adv. Mater.* **2005**, *17*, 1999−2003.

(18) Park, S.; Ruoff, R. S. Chemical methods for the production of graphenes. *Nat. Nanotechnol.* **2009**, *4*, 217−224.

(19) Rao, C. N. R.; Sood, A. K.; Subrahmanyam, K. S.; Govindaraj, A. Graphene: The New Two-Dimensional Nanomaterial. *Angew. Chem., Int. Ed.* **2009**, *48*, 7752−7777.

(20) Ferrari, A. C.; Bonaccorso, F.; Fal'ko, V.; Novoselov, K. S.; Roche, S.; Bøggild, P.; Borini, S.; Koppens, F. H. L.; Palermo, V.; Pugno, N.; Garrido, J. A.; Sordan, R.; Bianco, A.; Ballerini, L.; Prato, M.; Lidorikis, E.; Kivioja, J.; Marinelli, C.; Ryhanen, T.; Morpurgo, A.; Coleman, J. N.; Nicolosi, V.; Colombo, L.; Fert, A.; Garcia-Hernandez, M.; Bachtold, A.; Schneider, G. F.; Guinea, F.; Dekker, C.; Barbone, M.; Sun, Z.; Galiotis, C.; Grigorenko, A. N.; Konstantatos, G.; Kis, A.; Katsnelson, M.; Vandersypen, L.; Loiseau, A.; Morandi, V.; Neumaier, D.; Treossi, E.; Pellegrini, V.; Polini, M.; Tredicucci, A.; Williams, G. M.; Hee Hong, B.; Ahn, J.-H.; Min Kim, J.; Zirath, H.; van Wees, B. J.; van der Zant, H.; Occhipinti, L.; Di Matteo, A.; Kinloch, I. A.; Seyller, T.; Quesnel, E.; Feng, X.; Teo, K.; Rupesinghe, N.; Hakonen, P.; Neil, S. R. T.; Tannock, Q.; Lofwander, T.; Kinaret, J. Science and technology roadmap for graphene, related two-dimensional crystals, and hybrid systems. *Nanoscale* **2015**, *7*, 4598−4810.

(21) Vallés, C.; Young, R. J.; Lomax, D. J.; Kinloch, I. A. The rheological behaviour of concentrated dispersions of graphene oxide. *J. Mater. Sci.* **2014**, *49*, 6311−6320.

(22) Wan, Y. J.; Zhu, P. L.; Yu, S. H.; Sun, R.; Wong, C. P.; Liao, W. H. Ultralight, super-elastic and volume-preserving cellulose fiber/graphene aerogel for high-performance electromagnetic interference shielding. *Carbon* **2017**, *115*, 629−639.

(23) Wan, Y. J.; Zhu, P. L.; Yu, S. H.; Sun, R.; Wong, C. P.; Liao, W. H. Graphene paper for exceptional EMI shielding performance using large-sized graphene oxide sheets and doping strategy. *Carbon* **2017**, *122*, 74−81.

(24) Wang, Z. C.; Wei, R. B.; Liu, X. B. Fluffy and Ordered Graphene Multilayer Films with Improved Electromagnetic Interference Shielding over X-Band. *ACS Appl. Mater. Interfaces* **2017**, *9*, 22408−22419.

(25) Jan, R.; Habib, A.; Akram, M. A.; Ahmad, I.; Shah, A.; Sadiq, M.; Hussain, A. Flexible, thin films of graphene-polymer composites for EMI shielding. *Mater. Res. Express* **2017**, *4*, 035605.

(26) Song, W. L.; Cao, M. S.; Lu, M. M.; Bi, S.; Wang, C. Y.; Liu, J.; Yuan, J.; Fan, L. Z. Flexible graphene/polymer composite films in

sandwich structures for effective electromagnetic interference shielding. *Carbon* **2014**, *66*, 67−76.
(27) Jiang, Q.; Liao, X.; Li, J.; Chen, J.; Wang, G.; Yi, J.; Yang, Q.; Li, G. Flexible thermoplastic polyurethane/reduced graphene oxide composite foams for electromagnetic interference shielding with high absorption characteristic. *Composites, Part A* **2019**, *123*, 310−319.
(28) Gupta, S.; Sharma, S. K.; Pradhan, D.; Tai, N. H. Ultra-light 3D reduced graphene oxide aerogels decorated with cobalt ferrite and zinc oxide perform excellent electromagnetic interference shielding effectiveness. *Composites, Part A* **2019**, *123*, 232−241.
(29) Zhang, N.; Wang, Z.; Song, R.; Wang, Q.; Chen, H.; Zhang, B.; Lv, H.; Wu, Z.; He, D. Flexible and transparent graphene/silver-nanowires composite film for high electromagnetic interference shielding effectiveness. *Science Bulletin* **2019**, *64*, 540−546.
(30) Lin, S. F.; Ju, S.; Shi, G.; Zhang, J. W.; He, Y. L.; Jiang, D. Z. Ultrathin nitrogen-doping graphene films for flexible and stretchable EMI shielding materials. *J. Mater. Sci.* **2019**, *54*, 7165−7179.
(31) Decher, G.; Hong, J. D.; Schmitt, J. Buildup of Ultrathin Multilayer Films by a Self-Assembly Process. 3. Consecutively Alternating Adsorption of Anionic and Cationic Polyelectrolytes on Charged Surfaces. *Thin Solid Films* **1992**, *210*, 831−835.
(32) Yang, Y. H.; Bolling, L.; Priolo, M. A.; Grunlan, J. C. Super Gas Barrier and Selectivity of Graphene Oxide-Polymer Multilayer Thin Films. *Adv. Mater.* **2013**, *25*, 503−508.
(33) Stevens, B.; Dessiatova, E.; Hagen, D. A.; Todd, A. D.; Bielawski, C. W.; Grunlan, J. C. Low-Temperature Thermal Reduction of Graphene Oxide Nanobrick Walls: Unique Combination of High Gas Barrier and Low Resistivity in Fully Organic Polyelectrolyte Multilayer Thin Films. *ACS Appl. Mater. Interfaces* **2014**, *6*, 9942−9945.
(34) Pierleoni, D.; Minelli, M.; Ligi, S.; Christian, M.; Funke, S.; Reineking, N.; Morandi, V.; Doghieri, F.; Palermo, V. Selective Gas Permeation in Graphene Oxide-Polymer Self-Assembled Multilayers. *ACS Appl. Mater. Interfaces* **2018**, *10*, 11242−11250.
(35) Kim, S.; Oh, J. S.; Kim, M. G.; Jang, W.; Wang, M.; Kim, Y.; Seo, H. W.; Kim, Y. C.; Lee, J. H.; Lee, Y.; Nam, J. D. Electromagnetic Interference (EMI) Transparent Shielding of Reduced Graphene Oxide (RGO) Interleaved Structure Fabricated by Electrophoretic Deposition. *ACS Appl. Mater. Interfaces* **2014**, *6*, 17647−17653.
(36) Lu, Z. G.; Ma, L. M.; Tan, J. B.; Wang, H. Y.; Ding, X. M. Transparent multi-layer graphene/polyethylene terephthalate structures with excellent microwave absorption and electromagnetic interference shielding performance. *Nanoscale* **2016**, *8*, 16684−16693.
(37) Kang, J.; Kim, D.; Kim, Y.; Choi, J. B.; Hong, B. H.; Kim, S. W. High-performance near-field electromagnetic wave attenuation in ultra-thin and transparent graphene films. *2D Mater.* **2017**, *4*, 025003.
(38) Li, Z.; Young, R. J.; Kinloch, I. A. Interfacial stress transfer in graphene oxide nanocomposites. *ACS Appl. Mater. Interfaces* **2013**, *5*, 456−463.
(39) Casiraghi, C.; Hartschuh, A.; Qian, H.; Piscanec, S.; Georgi, C.; Fasoli, A.; Novoselov, K. S.; Basko, D. M.; Ferrari, A. C. Raman Spectroscopy of Graphene Edges. *Nano Lett.* **2009**, *9*, 1433−1441.
(40) Stauffer, D.; Aharony, A. *Introduction to Percolation Theory*; Taylor and Francis: London, 1994; p 175.
(41) Chatterjee, S.; Nafezarefi, F.; Tai, N. H.; Schlagenhauf, L.; Nüesch, F. A.; Chu, B. T. T. Size and synergy effects of nanofiller hybrids including graphene nanoplatelets and carbon nanotubes in mechanical properties of epoxy composites. *Carbon* **2012**, *50*, 5380−5386.
(42) Pike, G. E.; Seager, C. H. Percolation and conductivity: A computer study. I. *Phys. Rev. B* **1974**, *10*, 14.
(43) Gao, J. F.; Li, Z. M.; Meng, Q. J.; Yang, Q. CNTs/UHMWPE composites with a two-dimensional conductive network. *Mater. Lett.* **2008**, *62*, 3530−3532.
(44) Zhao, S. A.; Chang, H. Y.; Chen, S. J.; Cui, J.; Yan, Y. H. High-performance and multifunctional epoxy composites filled with epoxide-functionalized graphene. *Eur. Polym. J.* **2016**, *84*, 300−312.
(45) Du, J. H.; Zhao, L.; Zeng, Y.; Zhang, L. L.; Li, F.; Liu, P. F.; Liu, C. Comparison of electrical properties between multi-walled carbon nanotube and graphene nanosheet/high density polyethylene composites with a segregated network structure. *Carbon* **2011**, *49*, 1094−1100.
(46) Wang, D. G.; Wang, X. G. Self-Assembled Graphene/Azo Polyelectrolyte Multilayer Film and Its Application in Electrochemical Energy Storage Device. *Langmuir* **2011**, *27*, 2007−2013.
(47) Wang, L.; Wang, W. C.; Fu, Y.; Wang, J. J.; Lvov, Y.; Liu, J.; Lu, Y. L.; Zhang, L. Q. Enhanced electrical and mechanical properties of rubber/graphene film through layer-by-layer electrostatic assembly. *Composites, Part B* **2016**, *90*, 457−464.
(48) Ambrosetti, G.; Johner, N.; Grimaldi, C.; Danani, A.; Ryser, P. Percolative properties of hard oblate ellipsoids of revolution with a soft shell. *Phys. Rev. E* **2008**, *78*, 061126.
(49) Li, J.; Kim, J. K. Percolation threshold of conducting polymer composites containing 3D randomly distributed graphite nanoplatelets. *Compos. Sci. Technol.* **2007**, *67*, 2114−2120.
(50) Marsden, A. J.; Papageorgiou, D. G.; Valles, C.; Liscio, A.; Palermo, V.; Bissett, M. A.; Young, R. J.; Kinloch, I. A. Electrical percolation in graphene-polymer composites. *2d Mater.* **2018**, *5*, 5.
(51) Huang, H. D.; Liu, C. Y.; Zhou, D.; Jiang, X.; Zhong, G. J.; Yan, D. X.; Li, Z. M. Cellulose composite aerogel for highly efficient electromagnetic interference shielding. *J. Mater. Chem. A* **2015**, *3*, 4983−4991.
(52) Cao, J. Y.; He, P.; Mohammed, M. A.; Zhao, X.; Young, R. J.; Derby, B.; Kinloch, I. A.; Dryfe, R. A. W. Two-Step Electrochemical Intercalation and Oxidation of Graphite for the Mass Production of Graphene Oxide. *J. Am. Chem. Soc.* **2017**, *139*, 17446−17456.
(53) Steurer, P.; Wissert, R.; Thomann, R.; Mülhaupt, R. Functionalized graphenes and thermoplastic nanocomposites based upon expanded graphite oxide. *Macromol. Rapid Commun.* **2009**, *30*, 316−327.

■ NOTE ADDED AFTER ASAP PUBLICATION

This paper was published ASAP on July 5, 2019, without incorporating some of the corrections from the authors. The corrected version was reposted on July 26, 2019.

DOI: 10.1021/acsanm.9b01126
ACS Appl. Nano Mater. 2019, 2, 5272−5281